



Ferrimagnetism as a consequence of cation ordering in the perovskite $\text{LaSr}_2\text{Cr}_2\text{SbO}_9$

Emily C. Hunter^a, Peter D. Battle^{a,*}, Robert Paria Sena^b, Joke Hadermann^b

^a Inorganic Chemistry Laboratory, University of Oxford, South Parks Road, Oxford OX1 3QR, UK

^b EMAT, University of Antwerp, Groenenborgerlaan 171, 2020 Antwerp, Belgium

ARTICLE INFO

Keywords:

Ferrimagnetism
Perovskite
Electron microscopy

ABSTRACT

A polycrystalline sample of $\text{LaSr}_2\text{Cr}_2\text{SbO}_9$ has been synthesised using a standard ceramic method and characterized by x-ray and neutron diffraction, magnetometry and electron microscopy. The perovskite-related compound crystallises in the triclinic space group $I\bar{1}$ with unit cell parameters of $a=5.5344(6)$ Å, $b=5.5562(5)$ Å, $c=7.8292(7)$ Å, $\alpha=89.986(12)^\circ$, $\beta=90.350(5)^\circ$ and $\gamma=89.926(9)^\circ$ at room temperature. The two crystallographically-distinct, six-coordinate cation sites are occupied by Cr^{3+} and Sb^{5+} in ratios of 0.868(2):0.132(2) and 0.462(2):0.538(2). Ac and dc magnetometry revealed that $\text{LaSr}_2\text{Cr}_2\text{SbO}_9$ is ferrimagnetic below 150 K with a magnetisation of $\sim 1.25 \mu_B$ per formula unit in 50 kOe at 5 K. Neutron diffraction showed that the cations on the two sites order in a G-type arrangement with a mean Cr^{3+} moment of $2.17(1) \mu_B$ at 5 K, consistent with a magnetisation of $1.32 \mu_B$ per formula unit.

1. Introduction

Perovskite compounds have the general formula ABO_3 where A is usually a relatively-large divalent or trivalent cation and B is a smaller transition-metal or p -block cation. Due to the chemical flexibility of the perovskite structure, the complexity of these compounds can be increased by the partial substitution of either or both of the cations A and B . This has led to the formation of “double”, “triple” and even “quadruple” perovskites – an example of the latter being $\text{CaCu}_3\text{Fe}_4\text{O}_{12}$ [1]. The large range of accessible compositions has given rise to a plethora of electronic and magnetic properties among perovskite compounds; materials are known that show long-range magnetic order, magnetoresistance [2], giant magnetocaloric effects [3], multiferroic behaviour [4], quantum spin liquid behaviour [5] and relaxor ferroelectricity [6]. One relatively new phenomenon is relaxor ferromagnetism, with $\text{La}_3\text{Ni}_2\text{SbO}_9$ being the prime example, although Cr-Doped $\text{Nd}_{0.5}\text{Ca}_{0.5}\text{MnO}_3$ has also been described as relaxor ferromagnet [7,8]. $\text{La}_3\text{Ni}_2\text{SbO}_9$, or $\text{La}_2\text{Ni}(\text{Ni}_{0.333}\text{Sb}_{0.667})\text{O}_6$, is a double perovskite that crystallises in the space group $P2_1/n$ and has two crystallographically-distinct, six-coordinate sites, B and B', that alternate in a 3D checkerboard pattern. One site is fully occupied by Ni^{2+} and the other is occupied by 33% Ni^{2+} and 67% Sb^{5+} . This creates an ordered-disordered structure as there is complete cation ordering across the B sites but the nickel and antimony cations are randomly distributed over the B' site. We originally prepared $\text{La}_3\text{Ni}_2\text{SbO}_9$ in the hope that

the imbalance of magnetic cations on the two sites would lead to ferrimagnetism, even if the superexchange interactions between pairs of Ni^{2+} cations were antiferromagnetic. Magnetometry measurements indicated that $\text{La}_3\text{Ni}_2\text{SbO}_9$ does show a spontaneous magnetisation below 105 K but in early neutron diffraction measurements no magnetic Bragg scattering associated with long-range magnetic order was observed. However, in a later study the intensity of the 011 reflection was seen to increase as a function of applied magnetic field [9]. HAADF-STEM and EDX measurements provided evidence of a varying Sb/Ni stoichiometry across the sample and the presence of Sb-rich regions. Thus it was postulated that there were magnetically isolated ferrimagnetic regions in $\text{La}_3\text{Ni}_2\text{SbO}_9$ whose moments only became co-aligned on the application of a magnetic field. In this way $\text{La}_3\text{Ni}_2\text{SbO}_9$ can be compared to relaxor ferroelectrics such as $\text{Pb}_3\text{MgNb}_2\text{O}_9$ where a net polarisation is only observed on the application of an electric field [10]. It is likely that the occurrence of relaxor ferromagnetic behaviour is dependent on many factors such as the extent of the cation ordering across the B sites, the degree of tilting and rotation of the BO_6 octahedra, which will affect the relative strengths of competing superexchange interactions, and the electronic structure of the magnetic cation. To investigate the relative importance of these factors we have previously synthesised $\text{La}_2\text{SrNi}_2\text{TeO}_9$ [11] and $\text{Sr}_3\text{Fe}_2\text{TeO}_9$ [12]. We found that both compounds are markedly different to $\text{La}_3\text{Ni}_2\text{SbO}_9$ with $\text{Sr}_3\text{Fe}_2\text{TeO}_9$ exhibiting a mixture of nano-twinned 1:1 and 2:1 cation-ordered regions

* Corresponding author.

E-mail address: peter.battle@chem.ox.ac.uk (P.D. Battle).

<http://dx.doi.org/10.1016/j.jssc.2017.01.024>

Received 6 January 2017; Received in revised form 26 January 2017; Accepted 29 January 2017

Available online 31 January 2017

0022-4596/ © 2017 The Authors. Published by Elsevier Inc.

This is an open access article under the CC BY license (<http://creativecommons.org/licenses/by/4.0/>).

while $\text{La}_2\text{SrNi}_2\text{TeO}_9$ predominantly behaves as spin glass but also contains regions of both C- and G-type magnetic order. In a continuation of this work we have now investigated the effect of replacing the σ -mediated superexchange interactions of $\text{La}_3\text{Ni}_2\text{SbO}_9$ with the solely π -mediated superexchange interactions present in the novel compound $\text{LaSr}_2\text{Cr}_2\text{SbO}_9$. In this paper we report on the structural and magnetic properties of $\text{LaSr}_2\text{Cr}_2\text{SbO}_9$ which have been determined using a combination x-ray and neutron diffraction, magnetometry and electron microscopy.

2. Experimental

A dark-brown, polycrystalline sample of $\text{LaSr}_2\text{Cr}_2\text{SbO}_9$ was synthesised using the traditional ceramic method. Stoichiometric quantities of SrCO_3 , Cr_2O_3 , Sb_2O_3 and pre-dried La_2O_3 were mixed and ground together for 30 min in an agate pestle and mortar and were then fired at 1100 °C for 16 h as a loose powder. The reaction mixture was then pelleted and heated at 1150 °C for 6 h, reground, and fired at 1150 °C for a further 24 h. It was then fired at 1250 °C, 1300 °C and 1350 °C for 48 h at a time. After each firing the sample was quench-cooled to room temperature and re-ground and re-pelleted. The progress of the reaction was monitored by powder x-ray diffraction and the reaction was deemed complete when there was no further change to the x-ray powder diffraction pattern.

X-ray powder diffraction data were collected in our laboratory on a PANalytical Empyrean diffractometer operating with $\text{Cu K}\alpha_1$ radiation over an angular range of $5 \leq 2\theta / ^\circ \leq 125$ at room temperature. Further powder diffraction data were collected on instrument I11 at the RAL Diamond Light Source. In the latter case, the sample was loaded into a 0.3 mm diameter borosilicate glass capillary and data were collected at room temperature by conducting a 30 min constant-velocity scan over an angular range of $0 \leq 2\theta / ^\circ \leq 150$ using the Multi-Analyser-Crystal (MAC) detector. By also measuring a silicon standard, the wavelength was found to be 0.8259 Å. The data were analysed using the Rietveld method [13], as implemented in the GSAS program suite [14], in order to determine the unit cell parameters. A cylindrical absorption correction of 2.74852, estimated using the Argonne X-ray Absorption calculator [15], was applied. Neutron powder diffraction data were collected on the GEM time-of-flight diffractometer at the ISIS spallation source at 5 K and 300 K. The data collected on banks 3–6, which were at angles of 34.96°, 63.62°, 91.30° and 154.40° to the incident beam, were refined simultaneously using the Rietveld method. A pseudo-Voigt function [16] was employed to model the peak shapes and the background was modelled using a 12-term shifted Chebyshev function for all banks. The sample was contained in an 8 mm diameter vanadium canister and a cylindrical absorption correction of 0.0124 was applied following use of the NIST neutron scattering and absorption calculator [17].

Specimens for electron microscopy were prepared by dispersing crushed $\text{LaSr}_2\text{Cr}_2\text{SbO}_9$ powder in ethanol and depositing a few drops of this solution on a copper grid covered with a holey carbon film. Selected-area electron diffraction (SAED) patterns were recorded with a Philips CM20 transmission electron microscope. High-resolution HAADF-STEM images and atomic resolution STEM-EDX maps were collected with a FEI Titan 80–300 “cubed” transmission electron microscope equipped with a Super-X detector and operated at 300 kV.

The dc and ac magnetometry data were collected on a Quantum Design SQUID magnetometer. The dc measurements were taken on warming the sample through the temperature range $5 \leq T/\text{K} \leq 300$ after cooling from room temperature to 5 K firstly in zero field (ZFC) and then in an applied field of 100 Oe (FC). The magnetisation per formula unit (f. u.) of the sample was also measured as a function of applied field at 5 K and 250 K over a field range of $-50 \leq H/\text{kOe} \leq 50$. The ac susceptibility was measured over the temperature range $5 \leq T/\text{K} \leq 300$ in a field of amplitude 3.5 Oe oscillating at frequencies of 1, 10, 100 and 1000 Hz.

3. Results

The X-ray diffraction pattern collected on the Empyrean diffractometer was initially analysed in the space group $I2/m$, as reported for $\text{Sr}_2\text{CrSbO}_6$ [18]. This resulted in a good fit with $\chi^2=2.331$ and $R_{\text{wp}}=6.5\%$. The perovskite phase was found to be contaminated with 1.20(2) wt% $\text{Sr}_2\text{Sb}_2\text{O}_7$. There was no evidence of strontium and lanthanum ordering over the A sites. Higher-resolution x-ray diffraction data were collected on instrument I11 at Diamond light source. A small shoulder was visible on the 200 reflection, which was identified as LaCrO_3 . Due the difficulty of separating the contributions of the two phases to the peak, a multi-phase refinement was carried out with the lattice parameters of LaCrO_3 being fixed at the values reported by Qasim et al. [19]. This showed the sample to be contaminated by 1.36(3) wt% LaCrO_3 and 1.58(2) wt% $\text{Sr}_2\text{Sb}_2\text{O}_7$. The lattice parameters of the principal phase refined to values of $a=5.52788(11)$ Å, $b=5.55186(10)$ Å, $c=7.84306(16)$ Å and $\beta=90.308(1)^\circ$ in $I2/m$. Partial cation ordering over the six-coordinate sites was identified with a $\text{Cr}^{3+}:\text{Sb}^{5+}$ ratio of 0.854(3): 0.146(3) on the 2d site and 0.479(3):0.521(3) on the 2a site.

The molar magnetic susceptibility of $\text{LaSr}_2\text{Cr}_2\text{SbO}_9$ is shown as a function of temperature in Fig. 1. There is a divergence of the ZFC and FC curves below 150 K, with the FC molar susceptibility increasing faster than the ZFC molar susceptibility on cooling. Both susceptibility curves reach a maximum before decreasing slightly on further cooling; the FC susceptibility reaches a maximum of $4.54 \text{ cm}^3 \text{ mol}^{-1}$ at 14 K and the ZFC reaches $2.24 \text{ cm}^3 \text{ mol}^{-1}$ at 40 K. $\chi^{-1}(T)$ cannot be considered to be linear below 250 K. Only the data in the temperature range $250 \leq T/\text{K} \leq 300$ were therefore fitted to the Curie-Weiss law, resulting in values of $2.5(2) \mu_B$ and $+62(10)$ K for the effective magnetic moment per Cr^{3+} cation and the Weiss constant, respectively. The high standard deviations are a consequence of the need to use only a limited temperature range in the data analysis. The field dependence of the magnetisation per formula unit is shown in Fig. 2. $M(H)$ is linear at 250 K, well above the magnetic transition temperature of 150 K, but non-linear at 5 K where a weak hysteresis is observed. The remanent magnetisation is $\sim 0.10 \mu_B$ per formula unit, the coercive field is 0.2 kOe and the saturation magnetisation is tending towards $\sim 1.25 \mu_B$ per formula unit. Below 150 K the ac susceptibility, see Fig. 3, is a function of frequency and complex. At each frequency, both the real and imaginary components show maxima at temperatures between 60 and 80 K; the frequency dependence is most obvious close to the temperature of the susceptibility maximum. The parameter $\Delta T_f/T_f \Delta(\log \omega)$ takes a value of 0.032, which is within the range expected for a canonical spin glass [20].

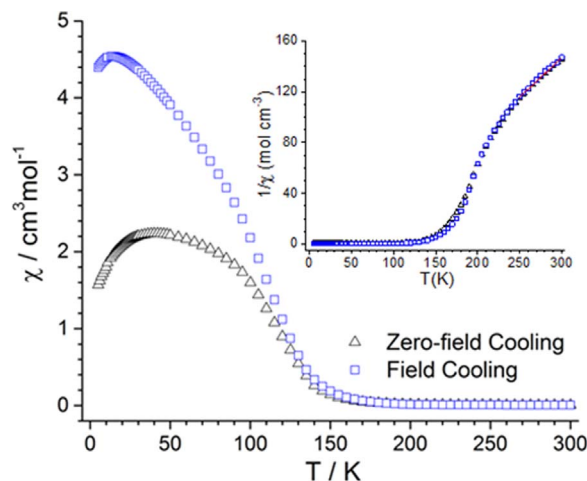


Fig. 1. The molar dc susceptibility and (inset) inverse susceptibility of $\text{LaSr}_2\text{Cr}_2\text{SbO}_9$ as a function of temperature.

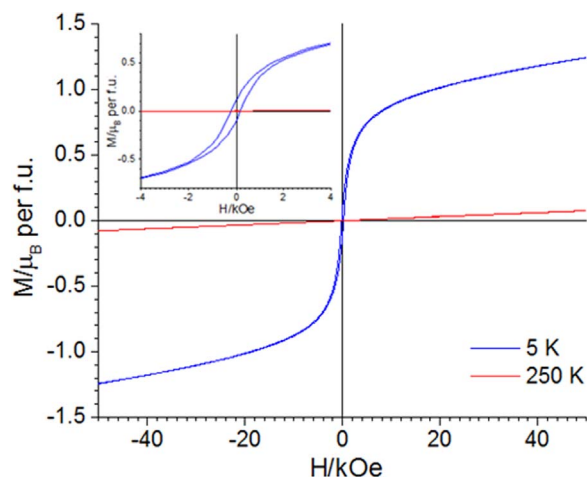


Fig. 2. Magnetic field dependence of the magnetisation per formula unit of $\text{LaSr}_2\text{Cr}_2\text{SbO}_9$ at 5 K (blue) and 250 K (red). (For interpretation of the references to color in this figure legend, the reader is referred to the web version of this article.)

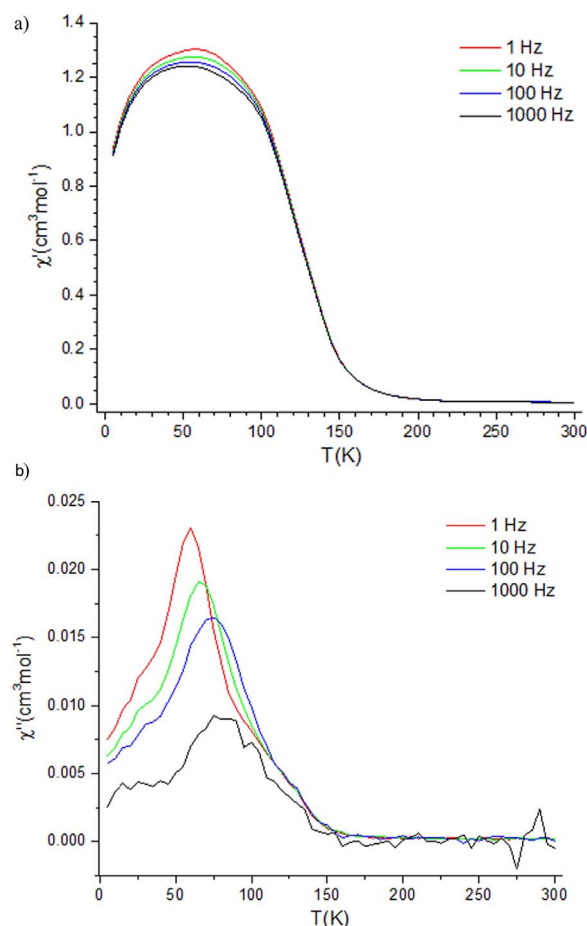


Fig. 3. Temperature and frequency dependence of the a) real and b) imaginary components of the ac susceptibility of $\text{LaSr}_2\text{Cr}_2\text{SbO}_9$ collected at 1 (red), 10 (green), 100 (blue) and 1000 (black) Hz. (For interpretation of the references to color in this figure legend, the reader is referred to the web version of this article.)

Neutron data collected on GEM were analysed using the Rietveld method. Although the data were initially refined in the space group $I2/m$, it was found that the $I\bar{1}$ space group gave a significantly better fit with χ^2 reduced from 6.515 to 3.698 for the 300 K data set and from 4.687 to 3.736 in the case of the 5 K data set. The space group $I\bar{1}$ is an alternative setting of $P\bar{1}$ in which the unit cell has twice the volume of the primitive cell. Use of the non-standard setting

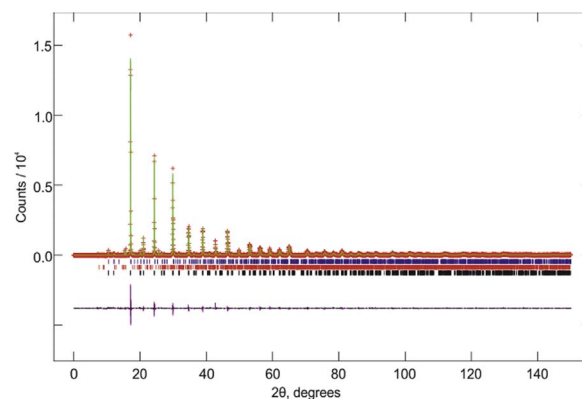


Fig. 4. Observed (red crosses) and calculated (green line) x-ray powder diffraction profiles recorded on I11 of $\text{LaSr}_2\text{Cr}_2\text{SbO}_9$ at room temperature using the $I\bar{1}$ space group model. Reflection markers are shown top to bottom for LaCrO_3 , $\text{Sr}_2\text{Sb}_2\text{O}_7$ and $\text{LaSr}_2\text{Cr}_2\text{SbO}_9$. (For interpretation of the references to color in this figure legend, the reader is referred to the web version of this article.)

facilitates comparison with other monoclinic and orthorhombic perovskites. The refined lattice parameters at room temperature are $a=5.5344(6)$ Å, $b=5.5562(5)$ Å, $c=7.8292(7)$ Å, $\alpha=89.986(12)^\circ$, $\beta=90.350(5)^\circ$, $\gamma=89.926(9)^\circ$ and at 5 K are $a=5.5239(5)$ Å, $b=5.5546(5)$ Å, $c=7.8081(7)$ Å, $\alpha=89.8703(18)^\circ$, $\beta=90.2482(18)^\circ$, $\gamma=90.103(5)^\circ$. Statistically significant distortions away from a monoclinic lattice are thus present at both temperatures. The x-ray diffraction data collected on I11 were re-analysed using the space group and oxygen coordinates derived from the neutron refinement and the final fit is shown in Fig. 4. The extent of the B site cation order remained effectively unchanged in this new model with the $\text{Cr}^{3+}:\text{Sb}^{5+}$ ratio on the 2g site being 0.868(2):0.132(2) and 0.462(2):0.538(2) on the 2f site. The level of contaminants also remained similar with 1.47(2) wt% $\text{Sr}_2\text{Sb}_2\text{O}_7$ and 1.36(3) wt% LaCrO_3 detected. From the neutron data, 1.80(4) wt% $\text{Sr}_2\text{Sb}_2\text{O}_7$ and 1.80(6) wt% LaCrO_3 were detected at 300 K.

The I11 data gave a much smaller error on the occupancies of the B sites than the GEM data and so the occupancies were fixed to those derived from the I11 data during the final analysis of both the 300 K and 5 K neutron datasets. The neutron diffraction patterns collected at 5 K and 300 K from the 34.96° and 91.30° banks are shown in Figs. 5 and 6. The neutron patterns collected on the 63.62° and 154.40° banks are included in Figs. S1 and S2 in the Supporting information. These four banks were refined simultaneously to determine the structural parameters, which are listed in Tables 1, 2, and selected bond lengths and angles are given in Tables 3, 4. The crystal structure of $\text{LaSr}_2\text{Cr}_2\text{SbO}_9$ at room temperature is shown in Fig. 7. Comparison of the neutron diffraction patterns collected at 5 K and 300 K shows that there is additional intensity in the 011 and 121 reflections at 5 K. Since this additional intensity is only apparent at high d -spacings it was assumed to be magnetic in origin and it could be accounted for by the addition of a G-type magnetically-ordered phase, see Fig. 8. Assuming that the whole sample orders antiferromagnetically, see below, the best fit was obtained when nearest-neighbour spins were set to be aligned antiparallel along [001] giving a refined Cr(III) moment of $2.17(1) \mu_B$. This gives an overall net magnetisation of $1.32 \mu_B$ per formula unit, which is in excellent agreement with the saturation magnetisation obtained from $M(H)$ at 5 K.

Selected-area electron diffraction (SAED) patterns were taken of the different zones, usually connected in tilt series, from many crystallites. Note that because the cell parameters and angles only deviate slightly from those of the cubic parent perovskite, it is impossible with transmission electron microscopy to differentiate geometrically between [100], [1-11], [111], [010], [1-1-1] and [11-1] ($= \langle 110 \rangle_p$, p refers to the parent perovskite cell), and also between [001], [1-10] and [110] ($= \langle 100 \rangle_p$). However, since all $\langle 110 \rangle_p$ and $\langle 100 \rangle_p$ ob-

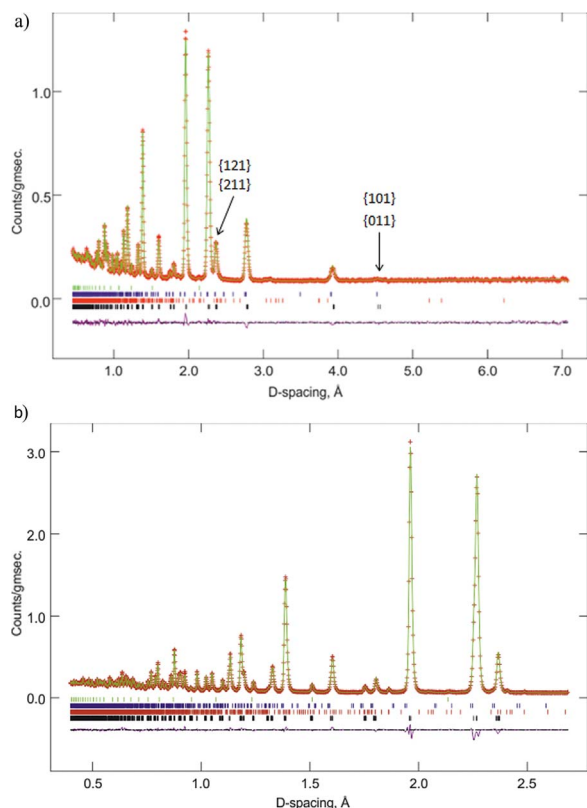


Fig. 5. Observed (red crosses) and calculated (green line) neutron powder diffraction profiles recorded on GEM of $\text{LaSr}_2\text{Cr}_2\text{SbO}_9$ at 300 K using the $I\bar{1}$ space group model using detector banks at a) 34.96° and b) 91.30° . Reflection markers are shown top to bottom for LaCrO_3 , the vanadium canister, $\text{Sr}_2\text{Sb}_2\text{O}_7$ and $\text{LaSr}_2\text{Cr}_2\text{SbO}_9$. The reflections that show magnetic scattering at 5 K in the 34.96° bank have been indexed. (For interpretation of the references to color in this figure legend, the reader is referred to the web version of this article.)

served showed the same body-centered patterns, we can conclude that the reflection conditions are $hkl: h+k+l=2n$, $Ok\bar{l}: k+l=2n$, $h0l: h+l=2n$, $hk0: h+k=2n$, $h: h=2n$, $0k0: k=2n$, $00l: l=2n$, consistent with the space group and unit cell derived from the neutron diffraction data. Representative patterns along the $\langle 110 \rangle_p$ and $\langle 100 \rangle_p$ zones are shown in Fig. 9. The underlined indices on these patterns represent one of the possible indexations using the supercell obtained from XRD.

The atomic-resolution HAADF-EDX map shown in Fig. 10 confirms that there is no ordering of Sr and La on the A site. On the B position there is an alternation in signal intensity for both Cr and Sb, but in a complementary way, as is also very clear from the combined map shown at the bottom right of the figure, i.e. both elements are present on both positions but Cr dominates one position and Sb the other. This is in agreement with the site occupancies determined from the x-ray diffraction data.

4. Discussion

$\text{LaSr}_2\text{Cr}_2\text{SbO}_9$ was synthesised in order to provide a perovskite analogue of $\text{La}_3\text{Ni}_2\text{SbO}_9$ that could be used in a comparison of the magnetic behaviour of a d^8 cation, where σ superexchange interactions are dominant, with that of a d^3 cation where π superexchange interactions are dominant. However, we have found that the structures are not directly comparable as $\text{La}_3\text{Ni}_2\text{SbO}_9$ crystallises in the monoclinic space group $P2_1/n$ whereas $\text{LaSr}_2\text{Cr}_2\text{SbO}_9$, or $\text{La}_{0.667}\text{Sr}_{1.333}\text{Cr}_{1.333}\text{Sb}_{0.667}\text{O}_6$, crystallises in the triclinic space group $I\bar{1}$. This group is uncommon amongst double perovskites but other examples include $\text{Ba}_2\text{LaRuO}_6$ [21] and $\text{Sr}_2\text{FeIrO}_6$ [22]. These space groups are similar in that they both introduce two crystallographi-

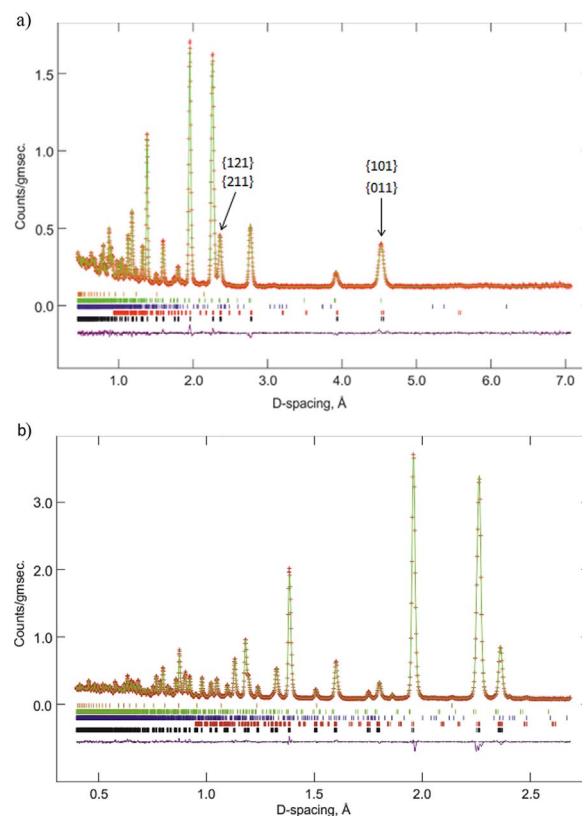


Fig. 6. Observed (red crosses) and calculated (green line) neutron powder diffraction profiles recorded on GEM of $\text{LaSr}_2\text{Cr}_2\text{SbO}_9$ at 5 K using the $I\bar{1}$ space group model using detector banks at a) 34.96° and b) 91.30° . Reflection markers are shown top to bottom for the vanadium canister, LaCrO_3 , $\text{Sr}_2\text{Sb}_2\text{O}_7$, G-type magnetic $\text{LaSr}_2\text{Cr}_2\text{SbO}_9$ and structural $\text{LaSr}_2\text{Cr}_2\text{SbO}_9$. The reflections in the 34.96° bank where magnetic scattering occurs have been indexed. (For interpretation of the references to color in this figure legend, the reader is referred to the web version of this article.)

cally-distinct six-coordinate cation sites and three independent oxygen positions, thus allowing the BO_6 octahedra to tilt about each of the three unit cell axes. However, the key difference is that the rotations of successive octahedra are out of phase along all three axes in $I\bar{1}$ whereas in $P2_1/n$ two of the rotations are out of phase and one is in-phase [23]. These tilts and rotations are smaller in $\text{LaSr}_2\text{Cr}_2\text{SbO}_9$, as is reflected by the B–O–B' bond angles given in Table 4. All three bond angles in $\text{LaSr}_2\text{Cr}_2\text{SbO}_9$ are larger than those in $\text{La}_3\text{Ni}_2\text{SbO}_9$, the average B–O–B' bond angles being 167.1° and 154.1° respectively at 300 K. The fact that the B–O–B' bond angles are much closer to 180° in $\text{LaSr}_2\text{Cr}_2\text{SbO}_9$ means that the antiferromagnetic superexchange interactions are likely to be much stronger than in $\text{La}_3\text{Ni}_2\text{SbO}_9$.

Another important difference between the two compounds is that there is full B-site ordering in $\text{La}_3\text{Ni}_2\text{SbO}_9$ whereas in $\text{LaSr}_2\text{Cr}_2\text{SbO}_9$ there is a partial mixing of the cations such that the 2g site is only 86.8% occupied by Cr^{3+} . This is not surprising given that there are smaller differences in charge and size between Cr^{3+} and Sb^{5+} than between Ni^{2+} and Sb^{5+} . This increased site disorder makes it more probable that a Cr^{3+} cation will be surrounded by 6 nearest-neighbour (NN) Cr^{3+} cations and also introduces the possibility of an antimony cation being surrounded by one of more NN antimony cations.

In a perovskite compound there are three types of superexchange interaction between six-coordinate cations. These are nearest-neighbour (J1), next-nearest neighbour (J2) and third nearest-neighbour (J3) superexchange interactions as illustrated in Fig. 11. To eliminate the effect of the J1 interaction one can look at the cation-ordered perovskites $\text{Sr}_2\text{CrSbO}_6$ and $\text{Ca}_2\text{CrSbO}_6$, where in both cases there is nearly complete 1:1 ordering of the B-site cations [24]. The mean B–O–B' bond angle of $\text{Sr}_2\text{CrSbO}_6$ is comparable to $\text{LaSr}_2\text{Cr}_2\text{SbO}_9$ at

Table 1
Structural parameters of LaSr₂Cr₂SbO₉ at room temperature.

Atom	Site	x	y	z	$U_{\text{iso}}/\text{\AA}^2$	Occupancy
Sr/La	4i	0.5014(17)	0.4992(10)	0.2469(11)	0.00886(20)	Sr: 0.6667 La: 0.3333
Cr/Sb1	2f	0	1/2	0	0.00115(13)	Cr: 0.462(2) Sb: 0.538(2)
Cr/Sb2	2g	1/2	0	0	0.00115(13)	Cr: 0.868(2) Sb: 0.132(2)
O1	4i	0.2577(12)	0.2587(14)	−0.0215(8)	0.0053(7)	1
O2	4i	0.2307(15)	0.7690(13)	0.0164(18)	0.0088(7)	1
O3	4i	0.4877(12)	0.0500(5)	0.2497(9)	0.0074(6)	1

R_{wp}=3.25%, R_p=2.52%, χ^2 =3.698

Space group I1: a=5.5344(6) Å, b=5.5562(5) Å, c=7.8292(7) Å, α=89.986(12)°, β=90.350(5)°, γ=89.926(9)°.

169.2°, while the mean B–O–B' bond angle of Ca₂CrSbO₆ is closer to that of La₃Ni₂SbO₉ at 152.47°. Sr₂CrSbO₆ is an A-Type antiferromagnet with T_N=12 K and Ca₂CrSbO₆ is a ferromagnet with T_C=16 K. LaSr₂Cr₂SbO₉ has a ferrimagnetic transition temperature of 150 K, which is too high a temperature to be attributable to the J3 interaction as demonstrated by CaCu₃Ti₄O₁₂, where the antiferromagnetic order below 25 K has been shown by x-ray absorption spectroscopy to originate from the Cu–O–Ti–O–Cu superexchange path [25]. The transition is also much higher in temperature than the J2-driven antiferromagnetic transition of Sr₂CrSbO₆, thus suggesting that the J1 interaction is dominant in this system. The strength of the J1 interaction is indicated by the transition temperature of LaCrO₃, 290 K [19]. The ferrimagnetic transition of LaSr₂Cr₂SbO₉ is lower due to the magnetic dilution of the B sites with ~33% diamagnetic Sb. It should be noted that the maximum in the FC curve of LaSr₂Cr₂SbO₉ at 14 K is close to the antiferromagnetic transition temperature of Sr₂CrSbO₆ so it is possible that this feature is caused by the increase in significance of J2 and J3 superexchange interactions.

La₂SrNi₂TeO₉ also has partial cation ordering with the 2c site having a Ni²⁺:Te⁶⁺ ratio of 0.83(3):0.17(3) and the 2d site a ratio of 0.50(3):0.50(3), which is very similar to the extent of the B-site cation order in LaSr₂Cr₂SbO₉ [11]. However, La₂SrNi₂TeO₉ is a spin glass with regions of C- and G-type cation order that are estimated to comprise of 19(2) wt% and 17(2) wt% of the sample, respectively. No Bragg reflections corresponding to C-type magnetic order were observed for LaSr₂Cr₂SbO₉. The mean B–O–B' bond angle in La₂SrNi₂TeO₉ at 300 K is 159.3°, which is between those of LaSr₂Cr₂SbO₉ and La₃Ni₂SbO₉. The smaller bond angle will weaken the J1 superexchange interaction in La₂SrNi₂TeO₉ and the fact that the superexchange interactions are σ rather than π mediated may be responsible for the different magnetic properties. The high degree of nanoscale [100][010] twinning that was found to occur in La₂SrNi₂TeO₉ might also be a factor.

However, LaSr₂Cr₂SbO₉ is not a simple ferrimagnet as the ac susceptibility clearly shows a frequency dependence of the transition

Table 2
Structural parameters of LaSr₂Cr₂SbO₉ at 5 K.

Atom	Site	x	y	z	$U_{\text{iso}}/\text{\AA}^2$	Occupancy
Sr/La	4i	0.4981(19)	0.4980(5)	0.2500(10)	0.00650(14)	Sr: 0.6667 La: 0.3333
Cr/Sb1	2f	0	1/2	0	0.00039(11)	Cr: 0.462(2) Sb: 0.538(2)
Cr/Sb2	2g	1/2	0	0	0.00039(11)	Cr: 0.868(2) Sb: 0.132(2)
O1	4i	0.2614(11)	0.26221(89)	−0.0263(7)	0.00643(58)	1
O2	4i	0.2441(11)	0.75633(81)	0.0234(5)	0.00421(52)	1
O3	4i	0.5054(13)	0.05112(26)	0.2501(8)	0.00485(30)	1

R_{wp}=3.14%, R_p=2.82%, χ^2 =3.736

Space group I1: a=5.5239(5) Å, b=5.5546(5) Å, c=7.8081(7) Å, α=89.8703(18)°, β=90.2482(18)°, γ=90.103(5)°.

Magnetic moment of Cr³⁺=2.17(1)μ_B**Table 3**
Selected bond lengths (Å) in LaSr₂Cr₂SbO₉ at room temperature and 5 K.

	Room temperature	5 K
Sr/La – O1	2.595(8)	2.568(4)
Sr/La – O1	2.712(12)	2.702(11)
Sr/La – O1	2.827(13)	2.839(11)
Sr/La – O2	2.602(8)	2.612(6)
Sr/La – O2	2.768(15)	2.671(10)
Sr/La – O2	2.776(14)	2.859(10)
Sr/La – O3	2.497(5)	2.483(3)
Sr/La – O3	2.721(12)	2.755(13)
Sr/La – O3	2.841(12)	2.796(13)
< Sr/La – O >	2.704	2.698
Cr/Sb1 – O1	1.964(7)×2	1.970(6)×2
Cr/Sb1 – O2	1.971(9)×2	1.967(6)×2
Cr/Sb1 – O3	1.980(7)×2	1.972(6)×2
< Cr/Sb1 – O >	1.972	1.970
Cr/Sb2 – O1	1.971(7)×2	1.976(6)×2
Cr/Sb2 – O2	1.973(9)×2	1.964(6)×2
Cr/Sb2 – O3	1.977(7)×2	1.974(6)×2
< Cr/Sb2 – O >	1.974	1.971

temperature akin to that of a spin glass. Furthermore, the refined Cr(III) moment at 5 K of 2.17(1) μ_B and the effective moment of 2.54(18) μ_B extracted from the Curie-Weiss fit are both lower than the expected values of ~2.5 μ_B and 3.7–3.9 μ_B [26]. Similar behaviour was seen in our study of La₃Ni₂SbO₉ [7,9]. In that case, a moment of 2.2(1) μ_B per Ni²⁺ cation was extracted from the Curie-Weiss fit, rather than the expected 2.83 μ_B, and no magnetic scattering was present in the neutron diffraction pattern [7]. In the present case we cannot place too much emphasis on the value of the effective moment because our data do not extend very far above the temperature of the ferrimagnetic transition. The moment refined from the neutron diffraction data is always expected to be reduced from the theoretical value of 3 μ_B by covalency in the Cr–O bonds, but the observed value is lower than in those reported in simple, comparable compounds, for example 2.63(3)

Table 4
Selected bond angles (°) in $\text{LaSr}_2\text{Cr}_2\text{SbO}_9$, $\text{La}_3\text{Ni}_2\text{SbO}_9$ [7] and $\text{La}_2\text{SrNi}_2\text{TeO}_9$ [11] at room temperature and 5 K.

$\text{LaSr}_2\text{Cr}_2\text{SbO}_9$	Room temperature	5 K
O1 – Cr/Sb1 – O2	93.02(28)×2	90.41(24)×2
O1 – Cr/Sb1 – O3	91.80(26)×2	91.29(17)×2
O2 – Cr/Sb1 – O3	91.3(5) ×2	91.40(20)×2
< O – Cr/Sb1 – O >	92.04	91.03
O1 – Cr/Sb2 – O2	91.94(28)×2	92.13(24)×2
O1 – Cr/Sb2 – O3	92.62(27)×2	90.14(18)×2
O2 – Cr/Sb2 – O3	90.2(5)×2	90.97(19)×2
< O – Cr/Sb2 – O >	91.59	91.08
Cr/Sb1 – O1 – Cr/Sb2	169.5(4)	166.90(26)
Cr/Sb1 – O2 – Cr/Sb2	168.5(4)	168.98(23)
Cr/Sb1 – O3 – Cr/Sb2	163.36(17)	163.35(11)
< Cr/Sb1 – O – Cr/Sb2 >	167.12	166.41
$\text{La}_3\text{Ni}_2\text{SbO}_9$		
Ni/Sb1 – O1 – Ni/Sb2	151.62(1)	151.3(3)
Ni/Sb1 – O2 – Ni/Sb2	155.62(1)	155.7(3)
Ni/Sb1 – O3 – Ni/Sb2	155.12(1)	154.7(2)
< Ni/Sb1 – O – Ni/Sb2 >	154.12	153.9
$\text{La}_2\text{SrNi}_2\text{TeO}_9$		
Ni/Te1 – O1 – Ni/Te2	159.7(4)	160.8(5)
Ni/Te1 – O2 – Ni/Te2	159.3(4)	157.4(5)
Ni/Te1 – O3 – Ni/Te2	158.8(2)	158.1(2)
< Ni/Te1 – O – Ni/Te2 >	159.3	158.8

μ_B in LaCrO_3 [27]. (However, we must point out that an even lower Cr(III) moment of 1.64(4) μ_B was reported for $\text{Sr}_2\text{CrSbO}_6$ [24].) One possible explanation for the frequency dependence of the transition temperature and the reduced value of the ordered moment is that the entire sample is not involved in long-range magnetic order due to the disruption caused by the presence of Sb–O–Sb NNs and variations in the relative strengths of competing superexchange interactions in the affected regions. We have previously argued that in $\text{La}_3\text{Ni}_2\text{SbO}_9$ there are magnetically isolated domains that only co-align to give long-range magnetic order on the application of an applied magnetic field. While the majority of $\text{LaSr}_2\text{Cr}_2\text{SbO}_9$ clearly exhibits long-range magnetic order that is detectable by neutron diffraction there may still be some magnetically isolated regions that do not contribute to the magnetic Bragg peaks. If we assume that there are regions of the sample that are not fully ordered and assign each ordered Cr(III) a moment of 2.6 μ_B

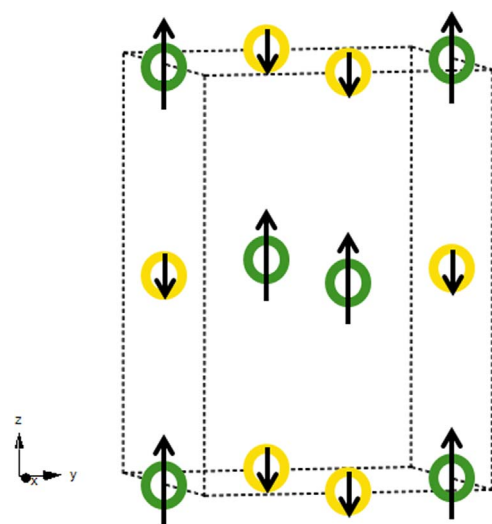


Fig. 8. The G-type antiferromagnetic structure adopted by $\text{LaSr}_2\text{Cr}_2\text{SbO}_9$.

then only 83.5(4) % of our sample is involved in the long-range G-type magnetic order. We propose that the remaining atomic moments behave in a glassy fashion and are thus responsible for the frequency dependence of the ac susceptibility.

5. Conclusion

Our attempts to make a ferrimagnet based on the unequal occupation by magnetic cations of two distinct but similar sites failed in the case of $\text{La}_3\text{Ni}_2\text{SbO}_9$ but they have succeeded in the case of $\text{LaSr}_2\text{Cr}_2\text{SbO}_9$, which orders ferrimagnetically below 150 K. However, not all of the Cr^{3+} ions are involved in the long-range magnetic order; the decoupled spins behave in a glass-like manner. It has been argued that, as a consequence of small differences in the crystal structures, stronger superexchange interactions are present in $\text{LaSr}_2\text{Cr}_2\text{SbO}_9$ than in $\text{La}_3\text{Ni}_2\text{SbO}_9$ and $\text{La}_2\text{SrNi}_2\text{TeO}_9$ and that the increase in strength facilitates the establishment of magnetic coherence in the former, despite the presence of cation disorder, rather than the formation of a dominant spin-glass phase, as occurs in $\text{La}_2\text{SrNi}_2\text{TeO}_9$, or the forma-

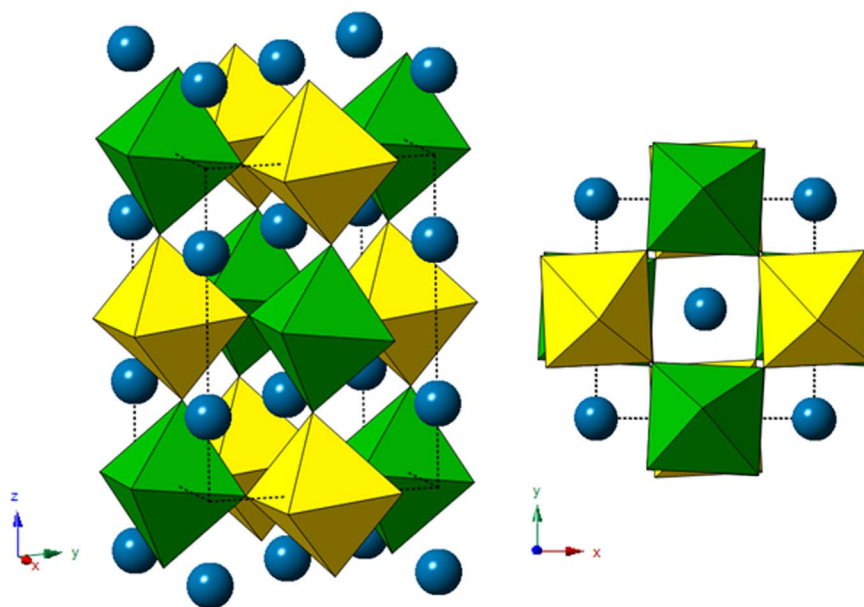


Fig. 7. The crystal structure of $\text{LaSr}_2\text{Cr}_2\text{SbO}_9$ generated from the structural parameters refined from the GEM data collected at 300 K. Green and yellow octahedra represent BO_6 and $\text{B}'\text{O}_6$ octahedra, respectively. The A cations are represented by blue circles. (For interpretation of the references to color in this figure legend, the reader is referred to the web version of this article.)

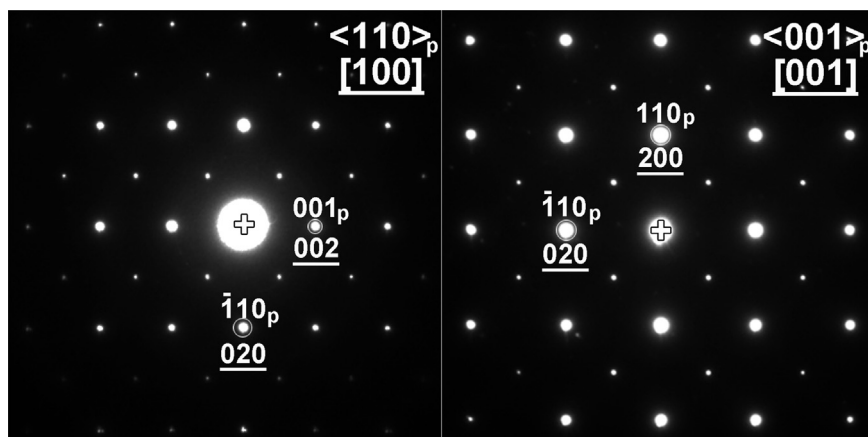


Fig. 9. Representative selective area electron diffraction (SAED) patterns taken of $\text{LaSr}_2\text{Cr}_2\text{SbO}_9$ crystallites along $\langle 100 \rangle_p$ and $\langle 110 \rangle_p$ zones (p refers to the perovskite subcell). The underlined indices represent one of the possible indexations in the supercell obtained from XRD.

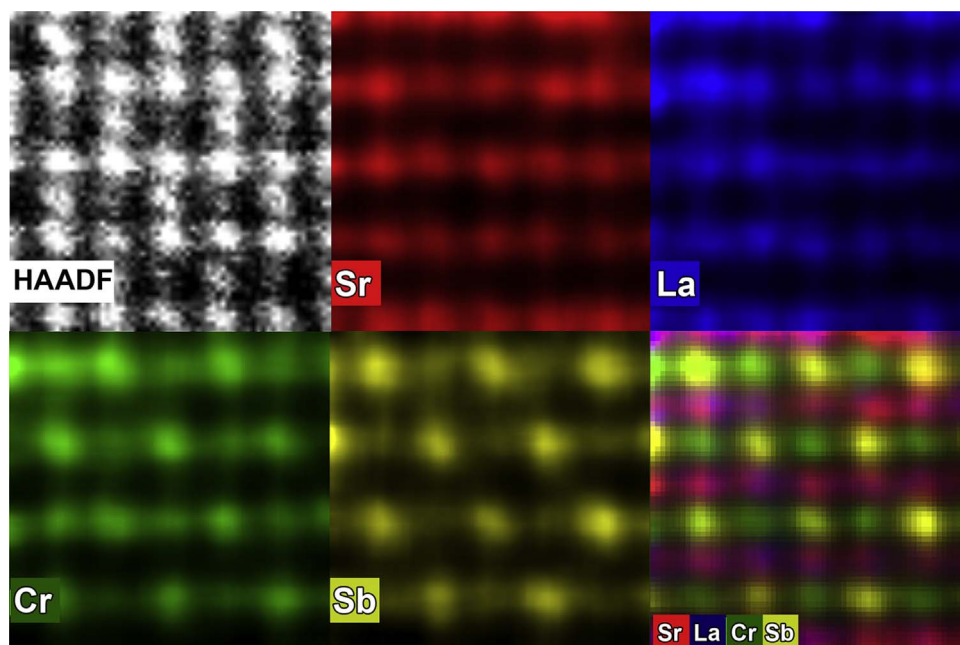


Fig. 10. Atomic resolution STEM-EDX map of $\text{LaSr}_2\text{Cr}_2\text{SbO}_9$ along a $[110]_p$ zone (p refers to the perovskite subcell). (For interpretation of the references to color in this figure legend, the reader is referred to the web version of this article.)

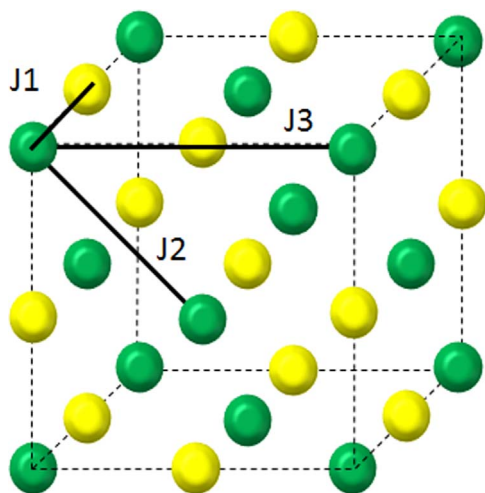


Fig. 11. Nearest neighbour (J1), next-nearest-neighbour (J2) and third nearest neighbour (J3) superexchange pathways between six-coordinate cation sites in a double perovskite.

tion of ferrimagnetic microdomains, as occurs in $\text{La}_3\text{Ni}_2\text{SbO}_9$. Thus it is appropriate to call $\text{LaSr}_2\text{Cr}_2\text{SbO}_9$ a frustrated ferrimagnet rather than a relaxor ferromagnet.

Acknowledgments

Experiments at the ISIS Pulsed Neutron and Muon Source were supported by the STFC. We are grateful to I. da Silva for the assistance provided at ISIS and to the EPSRC for financial support under Grant EP/M018954/1. We also thank Diamond Light Source Ltd (EE13284) for the award of beamtime.

Appendix A. Supporting information

Supplementary data associated with this article can be found in the online version at [doi:10.1016/j.jssc.2017.01.024](https://doi.org/10.1016/j.jssc.2017.01.024).

References

- [1] I. Yamada, M. Murakami, N. Hayashi, S. Mori, Inverse charge transfer in the quadruple perovskite $\text{CaCu}_3\text{Fe}_4\text{O}_{12}$, *Inorg. Chem.* 55 (2016) 1715–1719.

- [2] J. Navarro, L.I. Balcells, F. Sandiumenge, M. Bibes, A. Roig, B. Martínez, J. Fontcuberta, Antisite defects and magnetoresistance in $\text{Sr}_2\text{FeMoO}_6$ double perovskite, *J. Phys.: Condens. Matter* 13 (2001) 8481.
- [3] J.K. Murthy, K.D. Chandrasekhar, S. Mahana, D. Topwal, A. Venimadhav, Giant magnetocaloric effect in $\text{Gd}_2\text{NiMnO}_6$ and $\text{Gd}_2\text{CoMnO}_6$ ferromagnetic insulators, *J. Phys. D: Appl. Phys.* 48 (2015) 355001.
- [4] M.P. Singh, K.D. Truong, P. Fournier, P. Rauwel, E. Rauwel, L.P. Carignan, D. Ménard, A radical approach to promote multiferroic coupling in double perovskites, *J. Magn. Magn. Mater.* 321 (2009) 1743–1747.
- [5] T. Dey, A.V. Mahajan, R. Kumar, B. Koteswararao, F.C. Chou, A.A. Omrani, H.M. Ronnow, Possible spin-orbit driven spin-liquid ground state in the double perovskite phase of $\text{Ba}_3\text{YIr}_2\text{O}_9$, *Phys. Rev. B* 88 (2013) 134425.
- [6] A.A. Bokov, Z.G. Ye, Recent progress in relaxor ferroelectrics with perovskite structure, *J. Mater. Sci.* 41 (2006) 31–52.
- [7] P.D. Battle, S.I. Evers, E.C. Hunter, M. Westwood, $\text{La}_3\text{Ni}_2\text{SbO}_9$: a relaxor ferro-magnet, *Inorg. Chem.* 52 (2013) 6648–6653.
- [8] T. Kimura, Y. Tomioka, R. Kumai, Y. Okimoto, Y. Tokura, Diffuse phase transition and phase separation in Cr-doped $\text{Nd}_{1/2}\text{Ca}_{1/2}\text{MnO}_3$: a relaxor ferromagnet, *Phys. Rev. Lett.* 83 (1999) 3940–3943.
- [9] P.D. Battle, M. Avdeev, J. Hadermann, The interplay of microstructure and magnetism in $\text{La}_3\text{Ni}_2\text{SbO}_9$, *J. Solid State Chem.* 220 (2014) 163–166.
- [10] P.K. Davies, M.A. Akbas, Chemical order in PMN-related relaxors: structure, stability, modification, and impact on properties, *J. Phys. Chem. Solids* 61 (2000) 159–166.
- [11] R. Paria Sena, J. Hadermann, C.-M. Chin, E.C. Hunter, P.D. Battle, Structural chemistry and magnetic properties of the perovskite $\text{SrLa}_2\text{Ni}_2\text{TeO}_9$, *J. Solid State Chem.* 243 (2016) 304–311.
- [12] Y. Tang, E.C. Hunter, P.D. Battle, R.P. Sena, J. Hadermann, M. Avdeev, J.M. Cadogan, Structural chemistry and magnetic properties of the perovskite $\text{Sr}_3\text{Fe}_2\text{TeO}_9$, *J. Solid State Chem.* 242 (2016) 86–95.
- [13] H.M. Rietveld, A profile refinement method for nuclear and magnetic structures, *J. Appl. Crystallogr.* 2 (1969) 65–71.
- [14] Larson, A.C., Von Dreele, R. B., Los Alamos Natl. Lab. Rep. LAUR 1994, 86-748.
- [15] Argonne National Laboratory Compute X-ray Absorption. (<http://11bm.xray.aps.anl.gov/absorb/absorb.php>).
- [16] W.I.F. David, Powder diffraction peak shapes. Parameterization of the pseudo-Voigt as a Voigt function, *J. Appl. Crystallogr.* 19 (1986) 63–64.
- [17] NIST Center for Neutron Research Neutron Attenuation and Activation. (<https://www.ncnr.nist.gov/instruments/bt1/neutron.html>).
- [18] A. Faik, J.M. Igartua, M. Gateshki, G.J. Cuello, Crystal structures and phase transitions of $\text{Sr}_2\text{CrSbO}_6$, *J. Solid State Chem.* 182 (2009) 1717–1725.
- [19] I. Qasim, P.E.R. Blanchard, S. Liu, B.J. Kennedy, M. Avdeev, Impact of Cu doping on the structure and electronic properties of $\text{LaCr}_{1-y}\text{Cu}_y\text{O}_3$, *Inorg. Chem.* 53 (2014) 2240–2247.
- [20] J.A. Mydosh, *Spin Glasses*, Taylor & Francis Ltd, London, 1993.
- [21] P.D. Battle, J.B. Goodenough, R. Price, The crystal structures and magnetic properties of $\text{Ba}_2\text{LaRuO}_6$ and $\text{Ca}_2\text{LaRuO}_6$, *J. Solid State Chem.* 46 (1983) 234–244.
- [22] P.D. Battle, G.R. Blake, T.C. Gibb, J.F. Vente, Structural chemistry and electronic properties of $\text{Sr}_2\text{FeIrO}_6$, *J. Solid State Chem.* 145 (1999) 541–548.
- [23] P.M. Woodward, Octahedral tilting in perovskites. I. geometrical considerations, *Acta Crystallogr. Sect. B* 53 (1997) 32–43.
- [24] M. Retuerto, M. Garcia-Hernandez, M.J. Martinez-Lope, M.T. Fernandez-Diaz, J.P. Attfield, J.A. Alonso, Switching from ferro- to antiferromagnetism in A_2CrSbO_6 (A = Ca, Sr) double perovskites: a neutron diffraction study, *J. Mater. Chem.* 17 (2007) 3555–3561.
- [25] M. Mizumaki, T. Saito, H. Shiraki, Y. Shimakawa, Orbital hybridization and magnetic coupling of the A-site Cu spins in $\text{CaCu}_3\text{B}_4\text{O}_{12}$ (B=Ti, Ge, and Sn) perovskites, *Inorg. Chem.* 48 (2009) 3499–3501.
- [26] K. Burger, *Coordination Chemistry: Experimental Methods*, Butterworth, London, 1973.
- [27] M. Tseggai, P. Nordblad, R. Tellgren, H. Rundlöf, G. André, F. Bourée, Synthesis, nuclear structure, and magnetic properties of $\text{LaCr}_{1-y}\text{Mn}_y\text{O}_3$ ($y=0, 0.1, 0.2$, and 0.3), *J. Alloy. Compd.* 457 (2008) 532–540.